A lumped parameter model of free expanding Plasma Focus

González J.[1], Barbaglia M.[2], Casanova F.[2], Clausse A[2].

[1]*CNEA-CONICET and Instituto Balseiro, 8402 Bariloche, Argentina*
[2]*CNEA-CONICET and Universidad Nacional del Centro, 7000 Tandil, Argentina*
E-mail: plademа@exa.unicen.edu.ar

Abstract— In this paper, a model of Plasma Focus without surrounding cathode containing the radial expansion of the current sheath is presented. This configuration has been increasingly used in recent miniature devices. The model, based on the snowplow approximation, was applied to calculate the voltage along the pinch in a small 300 J device, showing good agreement with the experiments. The results can be useful in the design of x-rays applications of Plasma-Focus devices.

Keywords: Plasma Focus, pinch plasma, open-cathode, modeling

Introduction

A Plasma Focus in a low pressure gas environment produces a hot (around 0.3-1 keV) and dense (around 10^{25} m^{-3}) transient plasma for some nanoseconds, inducing ionization by means of a high pulsed voltage between a pair of coaxial cylindrical electrodes. The hot plasma is the result of the time evolution of the electrical discharge that travels along the coaxial electrodes. The discharge starts over the insulator separating the electrodes, and then the plasma sheath take-off axially accelerated by the magnetic field generated by the current itself. After the current sheath runs over the open end of the central electrode, the plasma becomes rapidly compressed into a small column resulting in very hot and dense plasma (pinch).

Recently, small Plasma-Focus devices were developed aiming to applications of the pulsed radiation emissions of the pinch (Soto et. al. 2001, Silva et. al. 2002, Moreno et. al 2003, Silva et. al. 2003, Soto et. al. 2008, Rout et. al. 2009). Miniature devices were constructed following a special configuration derived from capillary discharges, where the surrounding cathode is replaced by a circular plate located at the base of the gun (Soto et. al. 2009, Barbaglia et. al 2009). This feature allows the

current sheath to expand freely during the run down. Often, these devices are designed following empirical practices based on accepted scale laws (Lee and Serban 1996, Soto et. al. 2009).

Several simple models were offered in the past to assist the design of Plasma-Focus devices. Mathuthu et. al. (1997) proposed a semiempirical model for in which the sheath has both radial and axial variation during the rundown phase, and both the damped current and pinch length are allowed to vary with time. Moreno et. al. (2000) derived a purely algebraic model capable of explaining the relation of the neutron production with the gas-filling pressure and the geometrical parameters of the device, based in the thermonuclear component of the fusion reaction.

More sophisticated theories were applied to describe in detail the kinematics of the current sheath. Moreno et. al. (2003) and Casanova et. al. (2005) presented a finite-element approximation of Plasma Focus discharges, which reproduced with very precisely the shape evolution of the sheath and the thermodynamics of the shock wave. Stepniewski (2004) proposed a numerical code based on the free points method to solve a set of non-ideal MHD equations including the kinetics of ionization.

Lumped parameters models were applied with excellent results, providing fast tools to assess the dynamic features of Plasma Foci operation. Lee S. (1989) proposed a model based in the snow-plow approximation of the MHD equations, which was further extended to the simulation of different types of devices. Siahpoush et. al. (2005) and Goudarzi et. al (2008) adapted Lee's model to the Filippov type plasma focus geometry. Gonzalez et. al. (2004) presented a lumped parameter model of Mather-type Plasma Focus based on plane pistons, which explained the experimental neutron production of numerous devices assuming a thermonuclear reaction mechanism in the pinch.

In order to predict x-rays and the beam-target component of neutron emissions, more complex models taking into account the generation of beams of electrons and ions should be developed. An important variable involved in the beam generations of charged particles is the voltage acting along the pinch, which can exceed several times the charging voltage due to the inductance variation during the final compression.

In the present article, an extension of Gonzalez et. al. (2004) lumped parameter model is presented, introducing the initial radial expansion of the current sheath. This feature is important in the modeling of Plasma Focus without surrounding cathode, which is an increasingly used configuration in miniature devices (Soto et. al. 2009, Barbaglia et. al 2009). The model is applied to calculate the voltage along the pinch in a small 300 J device, showing good agreement against the experiments.

Description of the model

Let us consider the coaxial plasma gun configuration shown in Fig. 1. The anode is a cylindrical bar whereas the cathode is a plate with a central circular hole. This configuration has been used with good results in recent miniature Plasma-Focus devices (Soto et. al. 2009, Barbaglia et. al 2009). Following Lee's snowplow approximation (Lee 1989), the discharge process is partitioned in three stages, run-down, run-over, and pinch compression, and the evolution of the current sheath is idealized by means of axial and radial shock-waves (Fig. 2).

In the run-down stage, the current sheet is represented by an annular piston moving forward in the axial direction and a planar cylinder moving outwards from the insulator. The length of the latter is variable and it is determined by the position of the

axial piston (Fig. 2). The mass and momentum equations of the axial plasma piston are:

$$\frac{dM_x}{dt} = \xi_x \rho_o \pi \left(R^2 - R_a^2\right) v_x \qquad (1)$$

$$\frac{d\left(M_x v_x\right)}{dt} = \frac{1}{2} l I^2 \quad (2)$$

where a parameter ξx is introduced to account for shape effects, v_x is the axial piston velocity, ρ_o the density of the stagnant gas ahead of the piston, R the position of the plasma cylinder moving outwards in the radial direction, and l is the linear inductance of the expanding current sheath:

$$l = \frac{\mu_0}{2\pi} \ln\left(\frac{R}{R_a}\right) \qquad (3)$$

The radial expansion is modeled by a planar cylinder whose length is determined by the axial piston (Fig. 2). The mass and momentum balances of the radial expansion are:

$$\frac{dM_R}{dt} = \xi_R \rho_o 2\pi R x v_R \quad (4)$$

$$\frac{d\left(M_R v_R\right)}{dt} = \frac{\mu_o I^2}{4\pi} \frac{x}{R} \quad (5)$$

Note that the logarithmic factor of Eq. (3) does not appear in Eq. (5), since the magnetic pressure is constant over the radial piston area. In Eq. (4), the parameter ξ_R is introduced to account for shape effects.

Assuming that the electric current flows at the backside of the sheet, the circuit equation is:

$$\frac{d}{dt}\left\{\left[L_e + lX\right]\frac{dQ}{dt}\right\} + \frac{Q}{C} = V_{sg} \quad (6)$$

where x is the position of the piston backside, L_e is the inductance of the external circuit, Q and C are the capacitor charge and capacity, and V_{sg} is the voltage drop on the spark gap that is modeled as (Bruzzone et. al. 1989):

$$V_S(t) = \frac{Q_0}{C}\frac{\left[1+\exp(-\alpha t_o)\right]}{1+\exp\left[\alpha(t-t_o)\right]} \qquad (7)$$

where α and t_o are constant parameters characteristic of the switch, and Q_0 the initial capacitor charge.

The run-over stage occurs after the sheath arrival at the anode's open end, where the magnetic field accelerates the plasma toward the axis. The radial collapse is modeled by a radially imploding cylinder whose length is the difference between the axial piston and the anode length (Fig. 2). The mass and momentum balances and the electrical circuit equation of the radial contraction are analogous to the corresponding radial expansion during the breakdown.

The thickness of the axial piston, δ_X, can be calculated regarding that the mass fraction trapped in the axial portion of the sheath is:

$$M_X = \rho_{cs} v_X = \rho_{cs}\pi(R_{ext}^2 - R_{\text{int}}^2)\delta_X \quad (8)$$

In Eq. (8), R_{ext} and R_{int} are the corresponding internal and external radii of the sheath, and the current sheath density ρ_{cs} is calculated assuming the Rankine-Hugoniot relation (Anderson 2006):

$$\frac{\rho_{cs}}{\rho_o} = \frac{(\gamma+1)}{(\gamma-1)+\frac{2}{M^2}} \qquad (9)$$

where M is the Mach number.

Similarly the thickness of the imploding piston, δ_R, is related to its mass by:

$$M_R = \rho_{cs} v_R = \rho_{cs} \pi \left[R^2 - (R-\delta_R)^2\right](x+\delta_x - z) \qquad (10)$$

Pinch model

The pinch compression starts when the front of the imploding cylinder reaches the axis (i.e., R-δ_R=0). The resulting cylinder can be treated as a small plasma column compressed by the Lorentz force, which adiabatically increases its internal pressure and temperature until a minimum radius is reached (Fig. 3). Representing the pinch as a rigid cylinder should be interpreted as an effective model of a train of micropinches caused by m=0 instabilities, which is what experimental observations suggest. The momentum balance inside the pinch cylinder is written as (Gonzalez et. al. 2004):

$$\frac{d}{dt}(\rho_p v_r R_p^2) = R_p\left[p_i - p_M\right] \quad (11)$$

where ρ_p is the pinch mass density, R_p and v_r are the pinch radius and its temporal derivative, p_M is the magnetic pressure:

$$p_M = \frac{\mu_o I^2}{8\pi^2 R^2} \quad (12)$$

and p_i the internal pinch pressure, which can be related to the pinch radius (Gonzalez et. al. 2004).

The instantaneous voltage drop along the pinch is produced by the inductance variation during the compression of the plasma column. Knowing the voltage drop between electrodes, V_e, the current and the inductance of the current sheath, L_{cs}, the pinch voltage is calculated as:

$$V_p = V_e - \frac{d(L_e + L_{cs})I}{dt} \qquad (13)$$

Results

In order to validate the model, the numerical results were compared with experimental measurements in a Plasma Focus with open cathode. Table I details the geometric and electrical parameters of the device (Barbaglia et. al. 2009). Systematic measurements of the pinch voltage dependence with the charging voltage were reported, including a study of the influence of the anode length, z. The experimental pinch voltage was obtained indirectly by processing the signals of current and interelectrode voltage, combined with estimations of the gun inductance.

The equations were solved using the FORTRAN LSODE subroutine package (Hindmarsh 1983). Fig. 4 shows the pinch evolution calculated for a 25 kV discharge over a 28 mm anode, where the velocity of the pinch radius, v_R, and the voltage along the pinch are depicted.

Fig. 5 shows the peak voltage along the pinch as function of the charging voltage, for each of the anode length used in the reference experiment. In spite of the dispersion of the data, it can be seen that the model follows quite well the trend using

a single set of shape parameters, $\xi_X = 0.5$ and $\xi_R = 0.6$, which was sufficient to explain the data measured on three different anode lengths.

The sensitivity of the results to variations of the shape parameters ξ_X and ξ_R was studied for the reference case (z = 28 mm, V_o = 25 kV), resulting:

$$\frac{\xi_X}{V_p}\frac{dV_p}{d\xi_X} = 0.075$$

$$\frac{\xi_R}{V_p}\frac{dV_p}{d\xi_R} = -0.048$$

which indicates that the model is robust respect to uncertainties of the shape parameters.

Figs. 6 and 7 show the calculated pressure dependence of the pinch voltage and pinch current, for different anode lengths. It can be seen the pinch current presents a maximum, which corresponds to the coincidence of the pinch with the peak discharge current. In turn, the pinch voltage always decreases with the charging pressure.

Fig. 8 shows the variation of the pinch voltage with the anode length, keeping constant the charging pressure. It can be seen that there is an optimum anode length for each pressure, which maximizes the pinch voltage. Finally, Fig. 9 shows the maximum voltage and the corresponding optimum anode length as function of the charging pressure. Both magnitudes decrease as the pressure increases. These results can be useful in the design of Plasma Focus devices for applications of the x-ray emissions, which are known to be associated with the acceleration of electrons in the pinch.

Conclusions

A model of an open-cathode Plasma-Focus device was presented. The calculations of the pinch voltage have been tested with available data at different charging voltages and anode lengths, showing good agreement. It should be noted that the numerical pinch duration should be interpreted as an effective value, since the present model represents the pinch as a single rigid cylinder, whereas experimental observations suggest the occurrence of a train of micropinches caused by m=0 instabilities (Liberman et. al. 1999). A two dimensional model capable to describe the axial structure of the pinch would be required for a systematic description of these effects. The model set out here offers a useful tool to calculate and design of open-cathode Plasma-Focus devices applied to production of pulsed beams of charged particles.

REFERENCES

Anderson J. D., Hypersonic and high-temperature gas dynamics, AIAA, Virginia, 2nd Ed., p. 38, 2006.

Barbaglia M., Bruzzone H., Acuña H., Soto L., Clausse A., Experimental study of the hard x-ray emissions in a Plasma Focus of hundreds of joules, Plasma Phys Contr. Fusion, **51**, 045001 (9pp), 2009.

Bruzzone H, Kelly H and Moreno C, On the effect of finite closure time of switches in electrical circuits with fast transient behavior, Am. J. Phys. **57,** 63, 1989.

Casanova F. , MorenoC. , ClausseA., Finite-elements numerical model of the current-sheet movement and shaping in coaxial discharges, Plasma Phys. Control. Fusion, **47**, 1239-1250, 2005.

Di Lorenzo F., Lazarte A., Vieytes R., Clausse A., Moreno C., Anales de la Asociación de Física Argentina (in spanish), **16**, 138-141, 2004.

Gonzalez J., Florido P., Bruzzone H., Clausse A., A lumped parameter model of plasma focus, IEEE Transactions on Plasma Science, **32**, 1383-1391, 2004.

Goudarzi S., Amrollahi R., Moghaddam R. S., A Model Based on Lumped Parameters for Filippov-type Plasma Focus Devices, J Fusion Energ **27**, 195–199, 2008.

Hindmarsh A., Odepack, a Systematized Collection of ODE Solvers, Scientific Committing (R. S. Stepleman et al. Eds.), Amsterdam, p. 64, 1983.

Lee S., “Technology of a small PF”, Proceedings of the Spring College on Plasma Physics, ICTP, Trieste, pp. 113–169 (1989).

Lee. S., Serban A., “Dimensions and Lifetime of the Plasma Focus Pinch”, IEEE Trans. Plasma Sci., **24**, 1101-1105, 1996.

Liberman M., De Groot J., Toor A., Spielman R., Physics of High-Density Z-Pinch Plasmas, Springer Verlag, New York, p. 127, 1999.

Mathuthu M., Zengeni T., Gholap A., The Three-Phase Theory for Plasma Focus Devices, IEEE Trans. Plasma Sci. **25**, 1382-1388, 1997.

Moreno C., Bruzzone H., Martínez J., Clausse A., Conceptual Engineering of Plasma Focus Thermonuclear Pulsors, IEEE Trans. On Plasma Science, **28**, 1735-1741, 2000.

Moreno C., Casanova F., Correa G., Clausse A., Experimental study and modeling of the plasma dynamics of magnetically driven shock waves in a coaxial tube, Plasma Phys. Control. Fusion, **45**, 1989-1999, 2003.

Rout R., Mishra P., Rawool A., Kulkarni L., Gupta S., Battery powered tabletop pulsed neutron source based on a sealed miniature plasma focus device, J. Phys. D: Appl. Phys. **41**, 205211 (5pp), 2008.

Shapiro A., The Dynamics and Thermodynamics of Compressible Fluid Flow, The Ronald Press Company, **I**, 112, 1953.

Siahpoush V., Tafreshi M., Sobhanian S., Khorram S., Adaptation of Sing Lee’s model to the Filippov type plasma focus geometry, Plasma Phys. Control. Fusion **47,** 1065–1075, 2005.

Silva P., Soto L., Moreno J., Sylvester G., Zambra M., Altamirano L., Bruzzone H., Clausse A., Moreno C., A Plasma Focus Driven by a Capacitor Bank of Tens of Joules, Rev. Sci. Instruments **73**, 2583, 2002.

Silva P., Moreno J., Soto L., Birstein L., Mayer R., Kies W., Neutron Emission from a Fast Plasma Focus of 400 Joules”, Applied Physics Letters **83**, 3269, 2003.

Soto L., Esaulov A., Moreno J., Silva P., Sylvester G., Zambra M., Nazarenko A., Clausse A., Transient Electrical Discharge in Small Devices, Phys. Plasma **8**, 2572, 2001.

Soto L., Silva P., Moreno J., Zambra M., Kies W., Mayer R., Clausse A., Altamirano L., Pavez C., Huerta L., Demonstration of neutron production in a table-top pinch plasma focus device operating at only tens of joules, J. Phys. D: Appl. Phys. **41,** 205215 (7pp), 2008.

Soto L., Pavez C., Moreno J., Barbaglia M., Clausse A., Nanofocus: an ultra-miniature pinch focus device with submillimetric anode operating at 0.1 J, Plasma Sources Sci. Techn. **18,** 015007 (5pp), 2009.

Stepniewski W., MHD numerical modeling of the plasma focus phenomena, Vacuum **76**, 51–55, 2004.

TABLE I

PARAMETERS OF THE EXPERIMENT AND THE MODEL

Symbol	Parameter	Value
C	Bank capacity	0.8 μF
V	Charging voltage	18-28 kV
L_e	External inductance	65 nHy
z	Anode length	2.3 to 3 cm
R_a	Anode radius	0.31 cm
p_o	Filling pressure	1.8 mbar
α	Characteristic frequency of the spark gap	350 ns^{-1}
t_o	Characteristic delay of the spark gap	400 ns
ξ_x	Axial shape parameter	0.5
ξ_R	Radial shape parameter	0.6

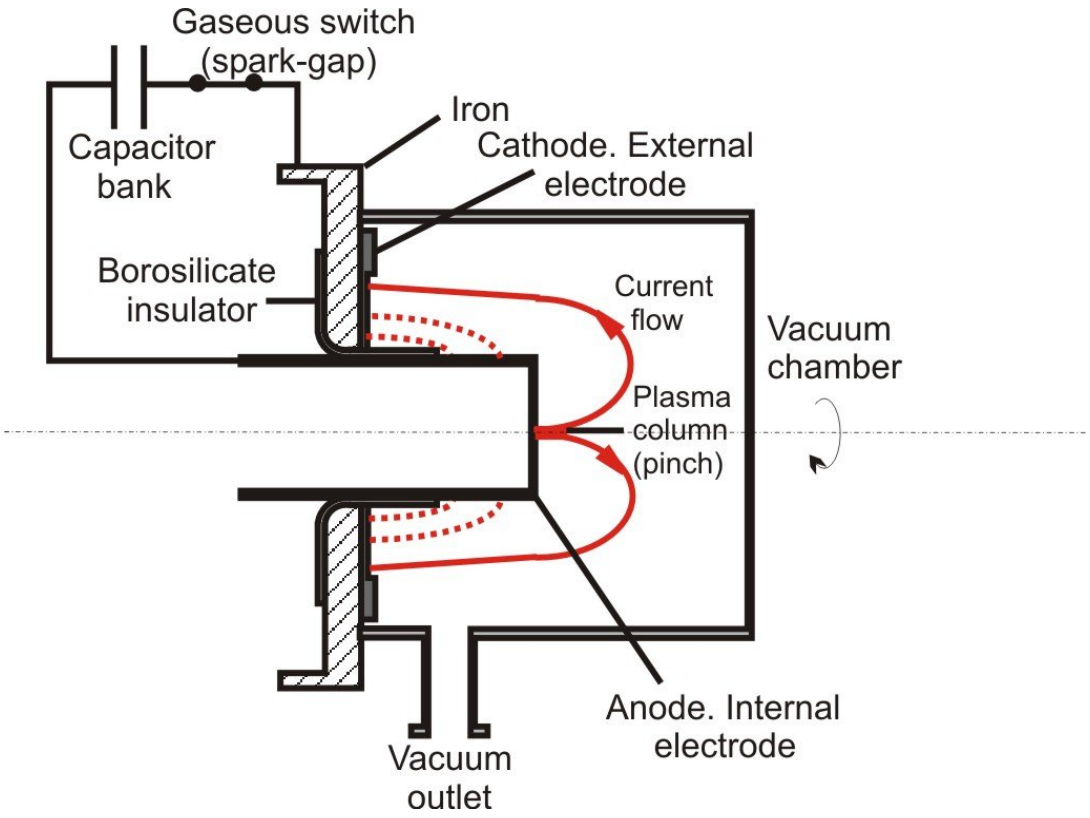

Figure 1. Diagram of an open-cathode Plasma Focus.

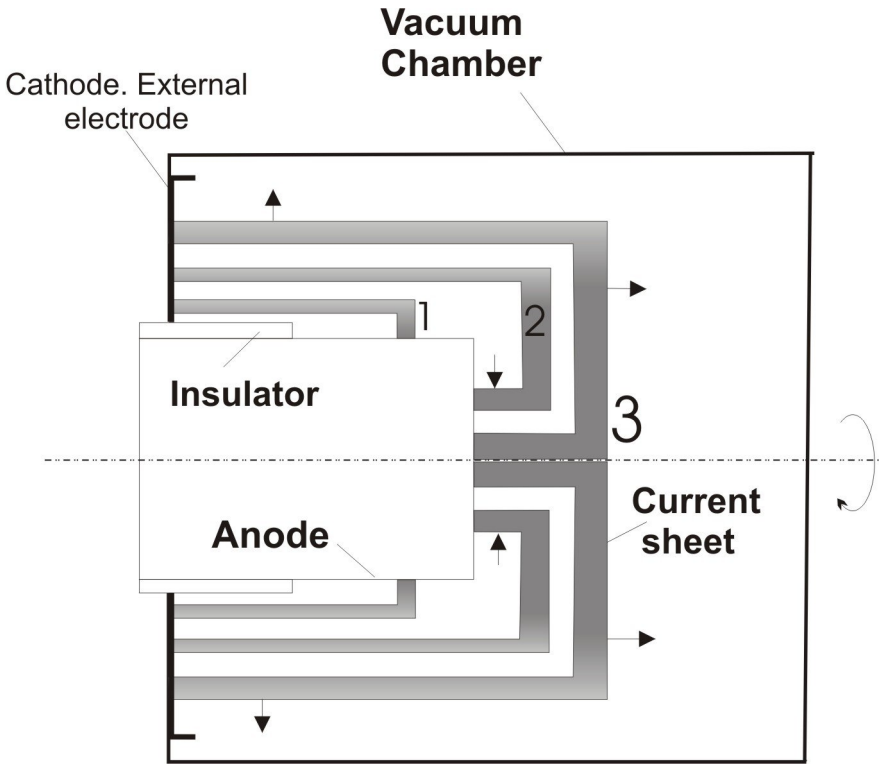

Figure 2. Lumped parameter model of an open-cathode Plasma Focus (1. Breakdown and run-down, 2. Run-over, 3. Pinch).

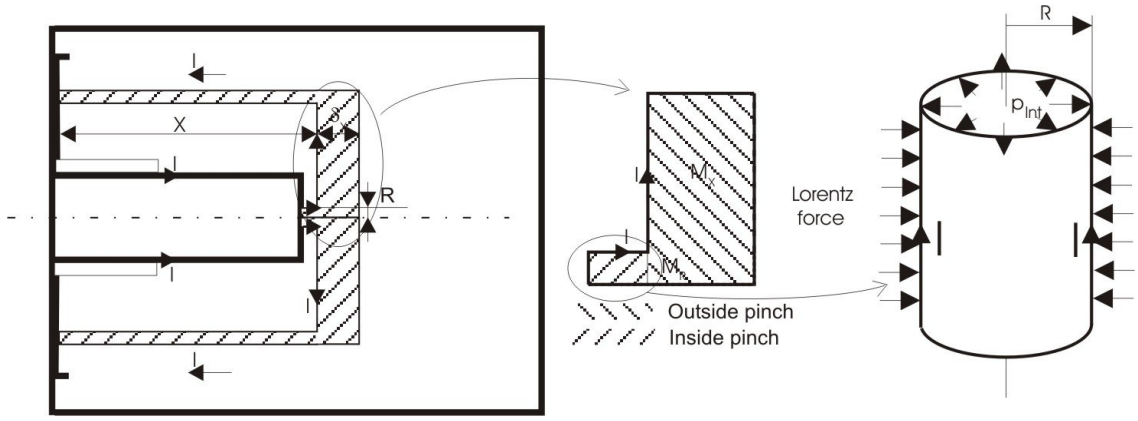

Figure 3. Diagram of the pinch model.

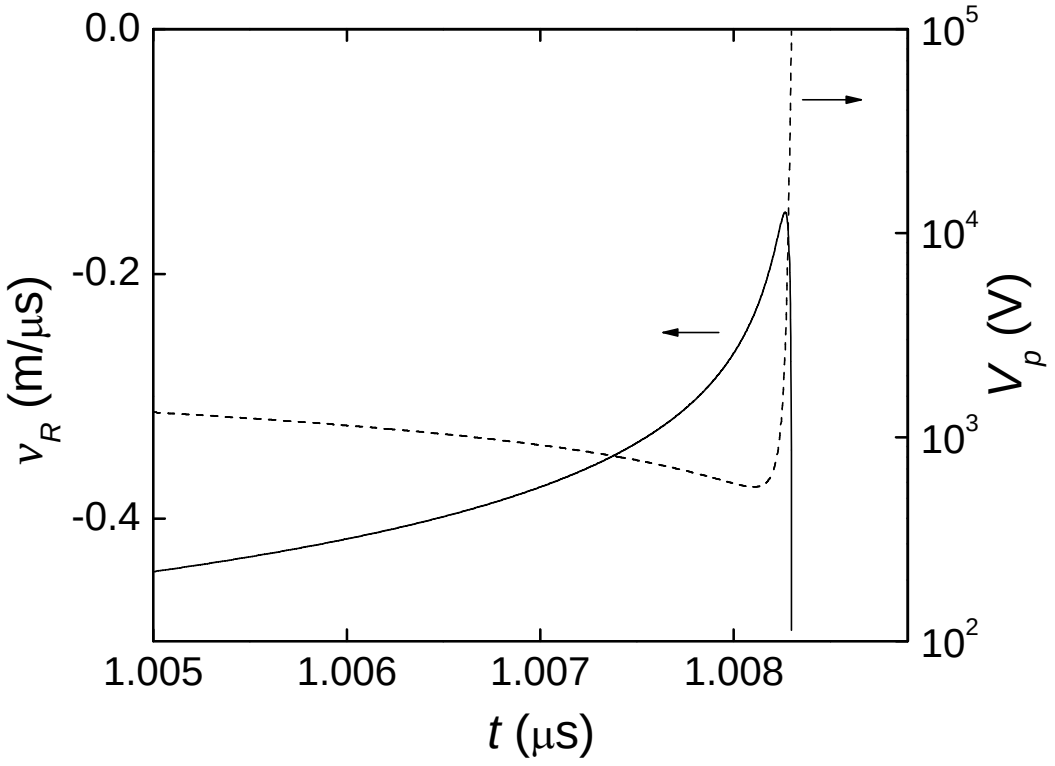

Figure 4. Numerical evolution of the velocity of the pinch and voltage-drop along the pinch.

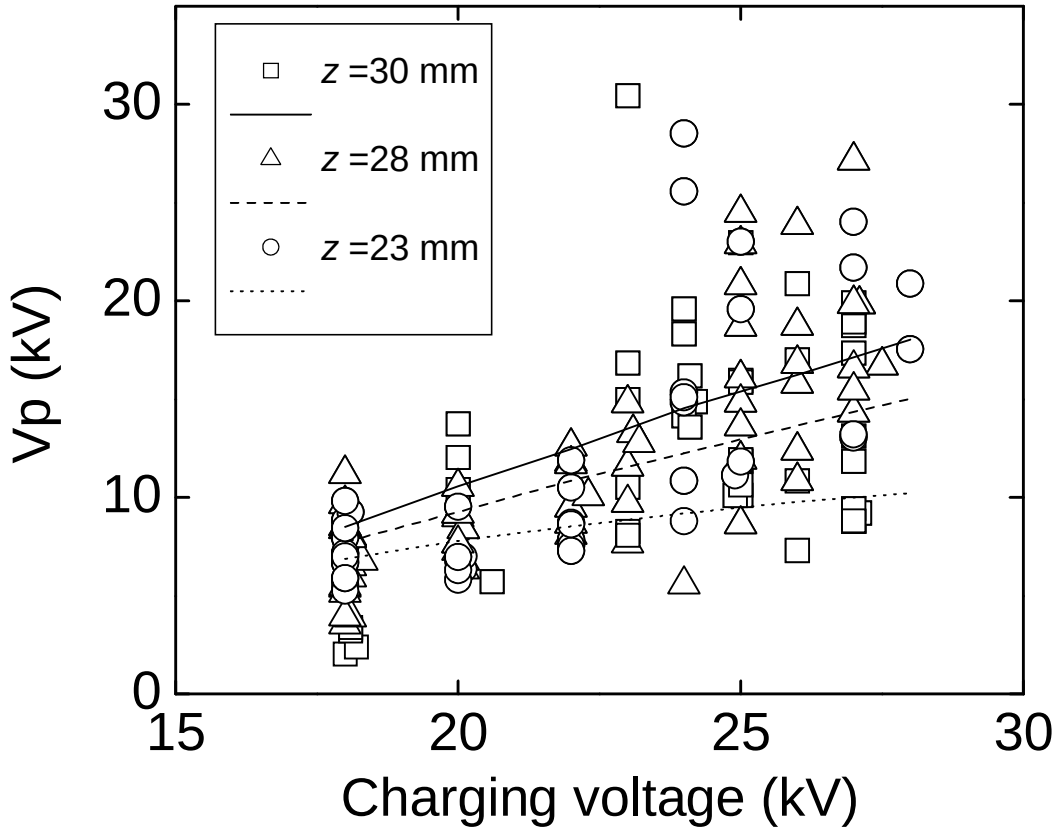

Figure 5. Peak voltage along the pinch measured and calculated for different charging voltages and different anode lengths.

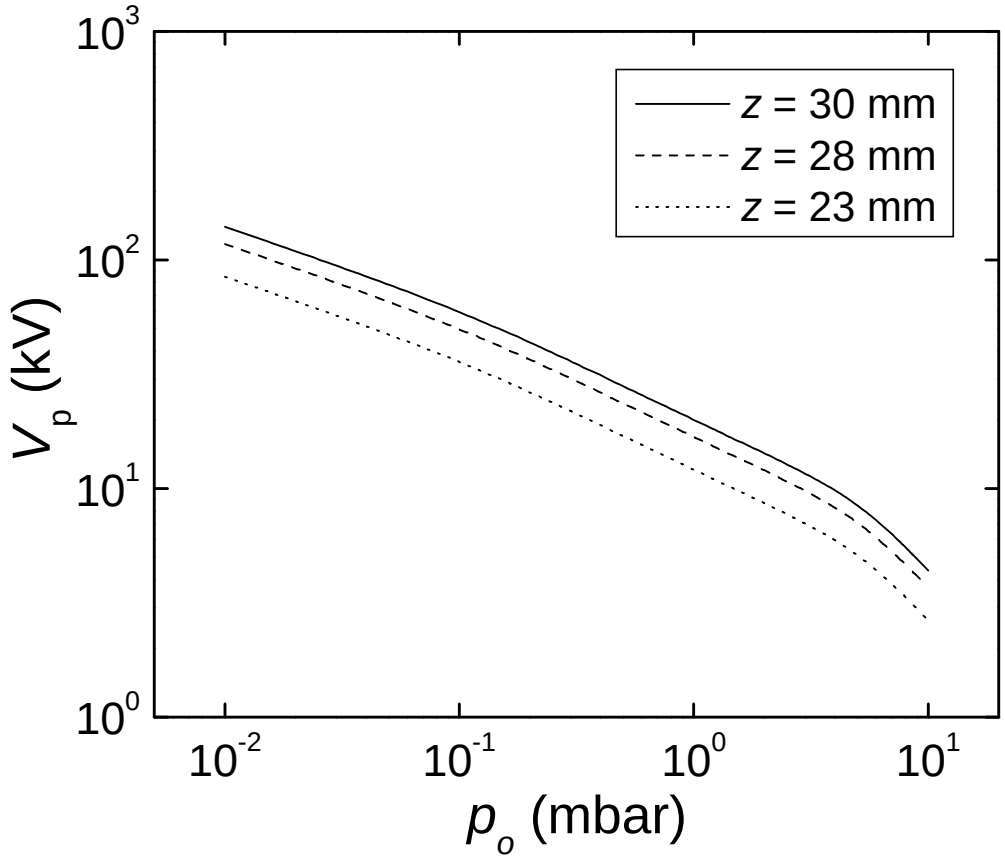

Figure 6. Charging-pressure dependence of the peak voltage along the pinch calculated for different anode lengths.

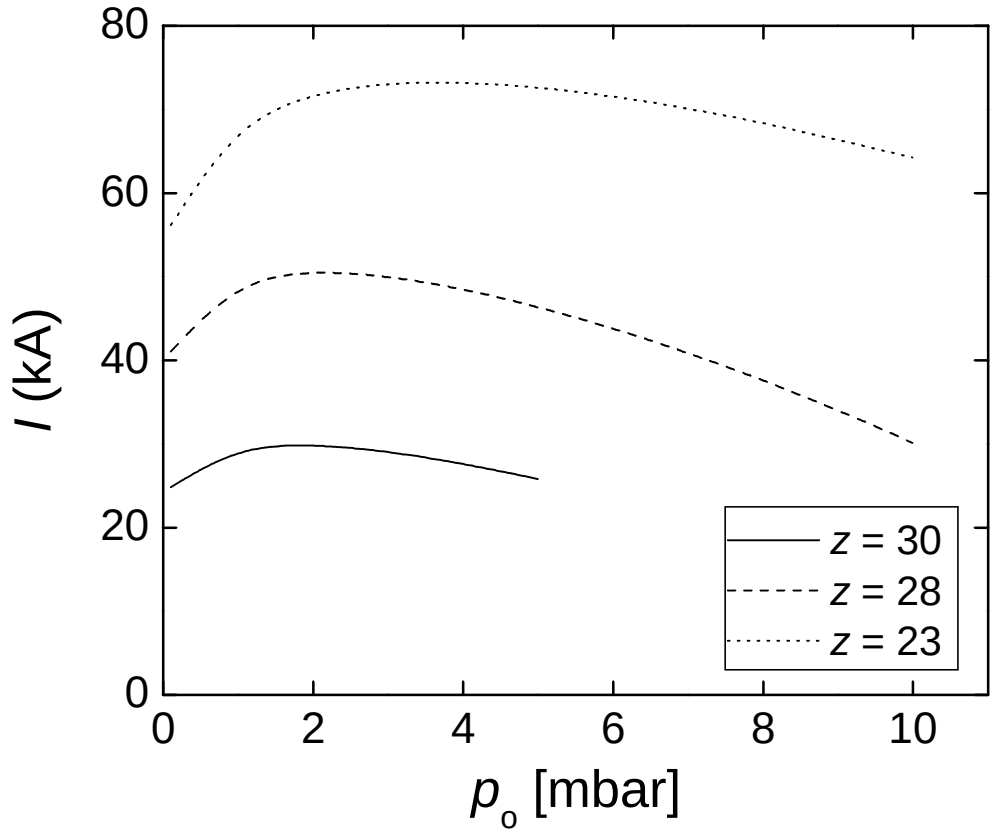

Figure 7. Charging-pressure dependence of the pinch current calculated for different anode lengths.

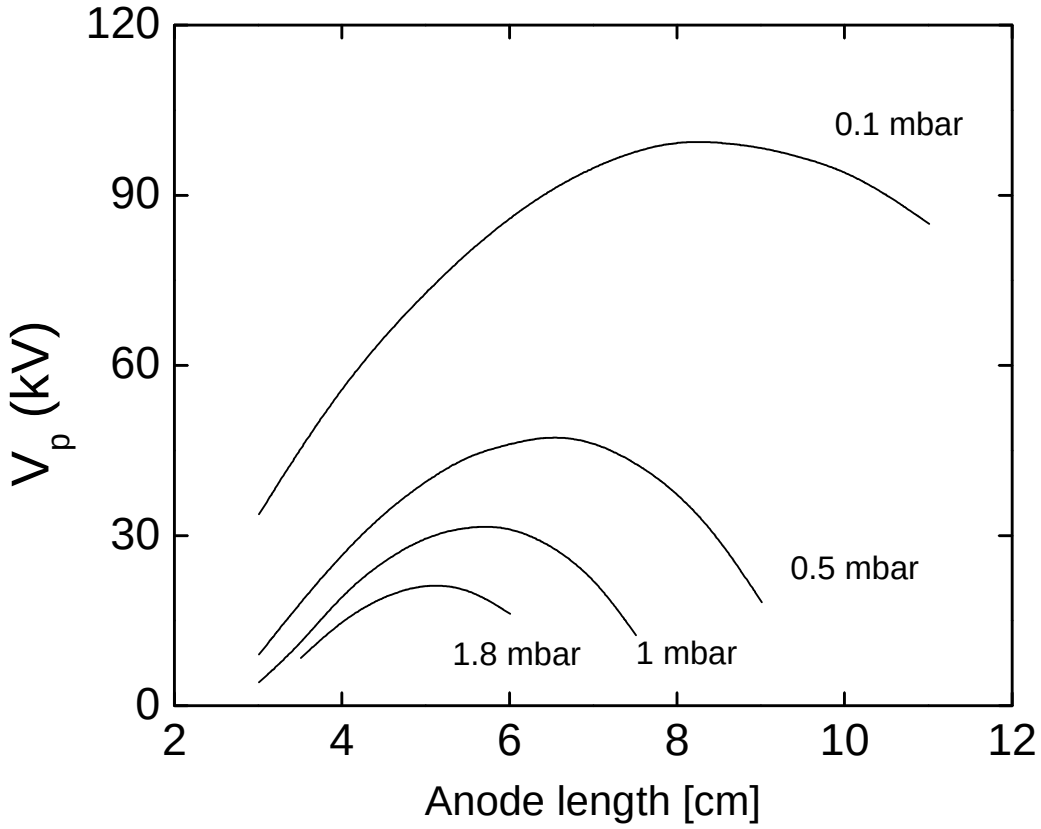

Figure 8. Peak pinch voltage as function of the anode length.

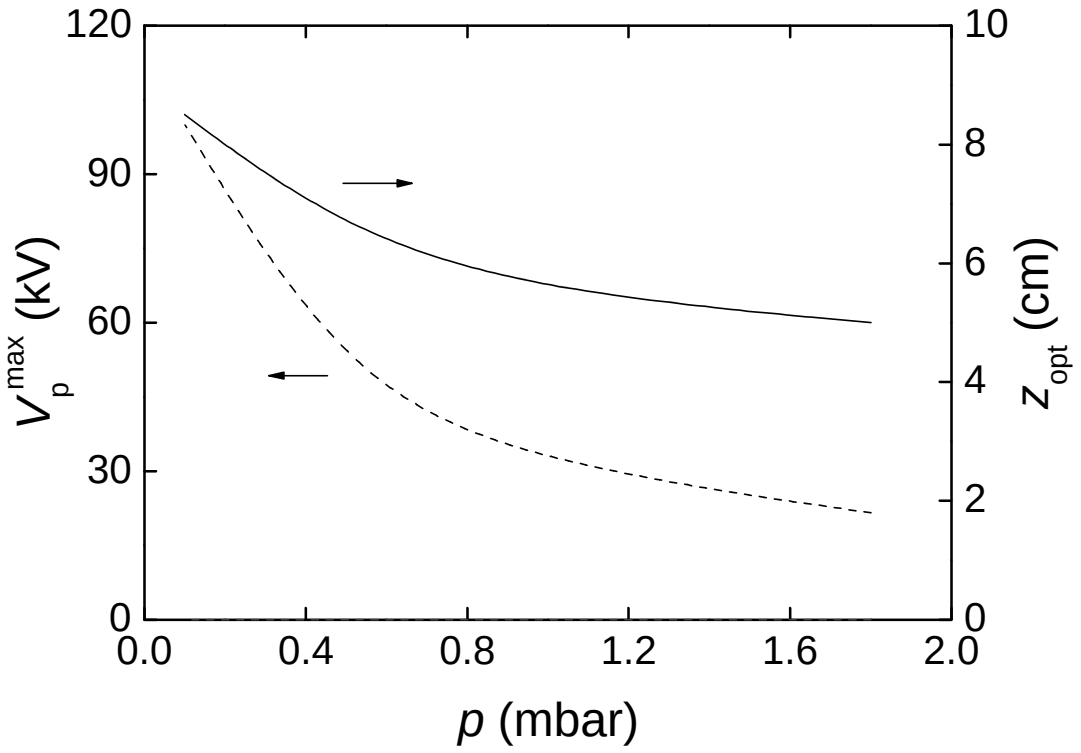

Figure 9. Optimum pinch voltage and the corresponding optimum anode length.